Organic Electronics 13 (2012) 90–97

Contents lists available at SciVerse ScienceDirect

Organic Electronics

journal homepage: www.elsevier.com/locate/orgel

Investigation of the energy transfer mechanism in OLEDs based on a new terbium β-diketonate complex

Alessandra Pereira [a], Hugo Gallardo [b,*], Gilmar Conte [b], Welber G. Quirino [c], Cristiano Legnani [c], Marco Cremona [c,d], Ivan H. Bechtold [a,*]

[a] Departamento de Física Universidade Federal de Santa Catarina – UFSC, 88040-900 Florianópolis, SC, Brazil
[b] Departamento de Química, INCT-Catálise, Universidade Federal de Santa Catarina – UFSC, 88040-900 Florianópolis, SC, Brazil
[c] Divisão de Metrologia de Materiais, Inmetro, Duque de Caxias, 252250-020 RJ, Brazil
[d] Departamento de Física, PUC-Rio, Rio de Janeiro, 22451-900 RJ, Brazil

ARTICLE INFO

Article history:
Received 28 February 2011
Received in revised form 8 October 2011
Accepted 14 October 2011
Available online 29 October 2011

Keywords:
OLED
Rare-earth compounds
Electroluminescent complexes
Energy transfer mechanisms

ABSTRACT

This study is focused on the contribution of radiative and non-radiative processes to the electroluminescence emission of OLEDs based on a new terbium(III) complex: {Tris(acetylacetonate)[1,2,5]thiadiazole[3,4-f][1,10]phenanthroline}terbium(III) or [Tb(ACAC)$_3$TDZP]. The effects of the energy transfer mechanism are discussed based on photoluminescence and electroluminescence measurements. The terbium complex showed an intense photoluminescence with high color purity in the green region, characteristics of the Tb(III) ion narrow line transitions. However, when used in a double-layer OLED its electroluminescence showed an orange broad band emission which can be attributed to the electrophosphorescence of the ligands and to an inefficient energy transfer from the organic ligand to the Tb(III) ion. Alternatively, devices with a Tb(III) complex acting as a dopant (7.6%) in a matrix of CBP used as the active layer showed an improvement in the energy transfer process, resulting in the appearance of the characteristic emission lines of the Tb(III) ion.

1. Introduction

Organic light-emitting diodes (OLEDs) have attracted great interest due to their potential application in the development of new optoelectronic components such as full-color and flat panel displays [1–3]. Nowadays, there is a range of luminescent materials available that can be applied in OLED technology, and thus by selecting an appropriate emitting compound it is possible to obtain the electroluminescence (EL) in the entire visible spectrum [4–7]. The EL of these devices is a result of the recombination of injected holes and electrons from the electrodes, which excites the emitting material. On the other hand, the photoluminescence (PL) results from the absorption of photons, exciting the compound to a higher energy state. In both cases the return to the fundamental energy level is accompanied by photon emission.

The majority of organic molecules exhibit spectrally broad emission bands, where the vibrational broadening difficult the achievement of the spectral purity required for full-color displays. These organic materials lead to an inherent limitation, where from simple spin statistical arguments one expects a ratio (3:1) of roughly three triplets to one singlet. Therefore, if only the singlet fraction is being used, their inner quantum efficiency is really limited to approximately 25%. The singlet excited state leads to fluorescence, while the triplet leads to phosphorescence. On the other hand, it is widely known that the specific spectroscopic properties of the trivalent rare earth ions make the RE^{3+} complexes to present additional advantages as emitting layers in electronic devices. The central ion can also emit due to intermolecular energy transfer from the

* Corresponding authors.
E-mail addresses: hugo@qmc.ufsc.br, hugo.gallardo@pq.cnpq.br (H. Gallardo), bechtold@fsc.ufsc.br (I.H. Bechtold).

1566-1199/$ - see front matter © 2011 Elsevier B.V. All rights reserved.
doi:10.1016/j.orgel.2011.10.007

triplet states of the ligands directly excited by excitons or photons, resulting in a theoretical upper limit close to 100%. In addition, the sharp emission bands of the rare earth ions are very suitable for full-color applications [1,8–10].

Generally, people working with RE^{3+} complexes define them as long time fluorescent or phosphorescent materials. From the lifetime point of view, with values spanning from hundreds of microseconds to milliseconds, they can be considered phosphorescent materials. Additionally, after the excitation (optical or electrical) the organic ligand triplet state is used to transfer energy to the central RE^{3+} ion identifying a phosphorescence process. Finally, the RE^{3+} transitions are generally prohibited from quantum rules (spin or Laport) and also in this case we can speak of phosphorescence. For all these reasons we can consider these complexes as phosphorescent emitters.

In particular, rare earth complexes with β-diketone ligands have attracted considerable attention as luminescent probes because of their high fluorescence emission efficiency caused by the high absorption coefficient of the β-diketone molecules and a high energy transfer rate to the central ion (known as the antenna effect) [11–13]. These compounds generally exhibit emission spectra dominated by narrow bands arising from intraconfigurational-$4F_j$ transitions centered on the RE^{3+} ions. The 4f–4f photoluminescence intensity is the result of a balance between absorption by the ligands, ligand-rare earth ion energy transfer rates, non-radiative decay and the radiative emission rates involved. Moreover, higher efficiency of energy transfer can be achieved when the appropriate organic ligand is selected [14]. J. Kido and co-workers showed the applicability of a $Tb(ACAC)_3$ complex as efficient EL layer, presenting the characteristic narrow lines of the Tb ion [15]. The incorporation of additional ligands in this complex, as phenanthroline (phen) [$Tb(ACAC)_3$(phen)] and 4-amino-antipyrine (AAP) [$Tb(ACAC)_3$AAP], resulted an enhancement of the energy transfer efficiency from the ligands to the central ion, promoting a gain of its emission intensity [16,17]. Likewise, we have incorporated the TDZP ligand and reported the synthesis, crystal structures and photophysical properties of the complex of tris-(thenoyltrifluoroacetonate)([1,2,5]thiadiazolo[3,4-f][1,10]phenanthroline) europium(III), which showed efficiently the characteristic red emission lines of the Eu(III) ion [18].

In recent years, β-diketonate rare-earth complexes have been incorporated into a variety of host molecules to fabricate co-doped devices [19,20] demonstrating an increase in the electroluminescence yield for rare earth devices. The basic condition required to fabricate efficient devices by doping phosphorescent molecules into a host matrix is that the triplet energy of the host matrix must be higher than that of the triplet energy of the phosphorescent dopant. This confine the triplet excitons generated in the recombination process to the guest molecule in the matrix.

In this study, the energy transfer mechanisms involved in the electroluminescence of the [$Tb(ACAC)_3$TDZP] are investigated using OLEDs. Our results demonstrate that the characteristic narrow emission lines of the Tb(III) ion are suppressed in an OLED double-layer structure using this Tb(III) complex due to an inefficient energy transfer from the ligand to the metallic ion, and only the broad bands of the ligand emission are observed. However, when the same Tb(III) complex is used as a dopant in a particular host matrix with an optimized concentration of 7.6%, the characteristic lines could be observed.

2. Experimental

The ligand [1,2,5]thiadiazolo[3,4-f][1,10]phenanthroline (TDZP) was prepared using a straightforward and efficient methodology, in four steps, from phenanthroline, as described in Ref. [21]. The synthesis of the Tb(III) complex used as the emitting material has been described in a recent publication [22]. OLEDs were assembled using the following: a heterojunction containing a double and triple-layer structure with copper phthalocyanine (CuPc) as the hole injection layer; N,N′-di(naphthalene-1-yl)-N,N′-diphenylbenzidine (NPB) as the hole-transporting layer; Tb(III)β-diketone complex, {Tris(acetylacetonate)[1,2,5]thiadiazolo[3,4-f][1,10]phenanthroline}terbium(III) or [$Tb(ACAC)_3$TDZP] as the transporting and emitting layer; and bipolar organic 4,4′-bis(carbazol-9-yl)biphenyl (CBP) as the host molecule. Finally, a 150 nm thick film of aluminum was deposited as the cathode. For the triple layered devices, the emitting molecular layer was prepared by co-evaporation of the Tb(III) complex and the CBP host molecule from two individual sources. The nominal concentration of Tb(III) complex ranged from 30% to 5% in the CBP matrix and the layer thickness was 50 nm. All the different layers where sequentially deposited in a high vacuum environment (Angstrom Engineering) by thermal evaporation onto ITO substrates with a sheet resistance of 8.1 Ω/ square. The fabricated devices are listed below with the corresponding layer thickness.

Double layer devices:

(I) ITO/NPB(40 nm)/Tb(ACAC)3TDZP(50 nm)/Al (150 nm)
(II) ITO/NPB(40 nm)/Gd(ACAC)3TDZP(50 nm)/Al (150 nm)

Triple-layer devices:

(III) ITO/CuPc(10 nm)/NPB(40 nm)/30%Tb(ACAC) 3TDZP:CBP(50 nm)/Al (150 nm)
(IV) ITO/CuPc(10 nm)/NPB(40 nm)/15%Tb(ACAC) 3TDZP:CBP(50 nm)/Al (150 nm)
(V) ITO/CuPc(10 nm)/NPB(40 nm)/7.6%Tb(ACAC) 3TDZP:CBP(50 nm)/Al (150 nm)
(VI) ITO/CuPc(10 nm)/NPB(40 nm)/5%Tb(ACAC) 3TDZP:CBP(50 nm)/Al (150 nm)
(VII) ITO/CuPc(10 nm)/MTCD(30 nm)/7,6%Tb(ACAC) 3TDZP:CBP(40 nm)/Al (150 nm)
(VIII) ITO/CuPc(10 nm)/MTCD(30 nm)/7,6%Gd(ACAC) 3TDZP:CBP(40 nm)/Al (150 nm)

The ITO substrates were initially cleaned by ultrasonification using a detergent solution, followed by toluene degreasing, and then cleaned again by ultrasonification with pure isopropyl alcohol. The base pressure was

6.6×10^{-5} Pa and during the evaporation the pressure was $\sim 10^{-4}$ Pa. The deposition rates for the organic compounds were in the range of 0.3–3.7 Å/s. The layer thickness was controlled *in situ* through a quartz crystal monitor and confirmed with a profilometric measurement. The fabricated devices had an active area of around 4 mm^2 and operated in forward bias voltage, with ITO as the positive electrode and Al as the negative electrode.

The electrical measurements were taken simultaneously with the brightness using a LabVIEW-based program, a Keithley 2240 and a calibrated radiometer/photometer (Newport Power Meter, model 1830-C). The photoluminescence and electroluminescence spectra were obtained on a Photon Technology International (PTI) fluorescence spectrophotometer.

3. Results and discussions

The optical properties of thermally-deposited thin films of the $Tb(ACAC)_3TDZP$ complex were characterized at room temperature by optical measurements through UV–Vis absorption and PL, the results are presented in Fig. 1. We can easily observe two main absorption peaks located at 256 and 292 nm. Reference [22] reports the absorption spectra of the free TDZP ligand and of the complex in acetonitrile solution. These data show that the Tb(III) complex presents the characteristic absorption bands of the TDZP ligand, indicating that the coordination with the Tb(III) ion does not have a significant influence on the energy levels ($\pi \rightarrow \pi*$) of the ligand. The ACAC ligand peaks are more difficult to assign being located at shorter wavelengths and superimposed with those of the TDZP ligand. The PL spectrum was obtained from a 50 nm-thick film of the Tb(III) complex thermally deposited on a quartz substrate. The excitation wavelength was $\lambda = 330$ nm. In the figure it is possible to verify the transitions from the $^5D_4$ state to the ^7F_j ($j = 6,5,4,3$) levels, with the following spectral lines: 488 nm ($^5D_4 \rightarrow {}^7F_6$), 546 nm ($^5D_4 \rightarrow {}^7F_5$), 584 nm ($^5D_4 \rightarrow {}^7F_4$) and 619 nm ($^5D_4 \rightarrow {}^7F_3$). The $^5D_4 \rightarrow {}^7F_5$ transition is the most intense and is thus responsible for the green emission.

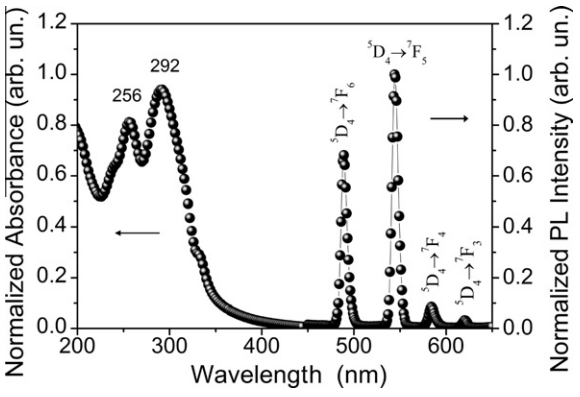

Fig. 1. Room temperature absorption and PL spectra of the Tb(III) complex 50 nm thin film deposited onto quartz substrate. For the PL, the excitation wavelength was $\lambda = 330$ nm.

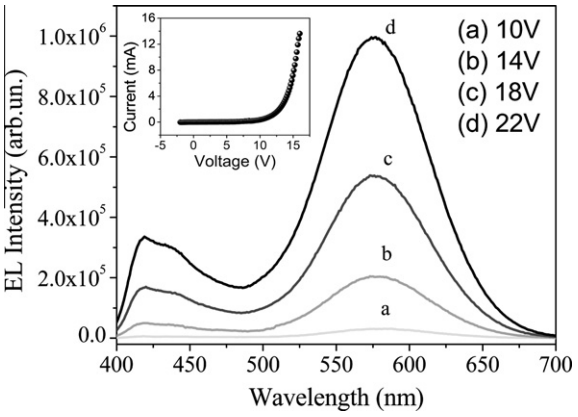

Fig. 2. EL spectra of the Device I as a function of bias voltage. The inset shows the $I \times V$ curve of this device.

The EL spectrum of Device I as a function of the bias voltage is shown in Fig. 2, where no characteristic narrow lines related to the Tb(III) ion are observed, but rather a two-component intense broad emission band appears. The first band, centered at 435 nm, can be identified as originating from the NPB emission [23]. Electrons injected from the cathode can be transported through the organic layers until the NPB where some recombination can occurs, thus allowing the formation of excitons followed by the NPB emission. The second band peak at around 580 nm can be attributed to the radiative transition from the triplet excited states of the ligands to its ground state, which is frequently reported as the electrophosphorescence of the ligands. The appearance of this broad band at 580 nm is a strong indication that the energy transfer mechanism from the ligands to the Tb central ion has a low efficiency. The inset in Fig. 2 shows the $I \times V$ curve, indicating typical diode behavior.

The energy transfer mechanism for the ligand's electrophosphorescence of Device I can be understood as follows. The holes and electrons injected into the emitting layer by the applied electric field will rater recombine on the emitter molecules to form singlet and triplet excitons, resulting in singlet and triplet excited states of the ligands. As discussed in the introduction, the triplet excited states directly generated by the carrier recombination contribute to increase the internal quantum efficiency. Fig. 3 illustrates the dissipation of the absorbed energy, where from the singlet excited state S_1 a radiative transition can occur to the ground state producing EL of the ligands, but usually a nonradiative decay through the intersystem crossing to the triplet state T_1 of the ligands is expected. At this point the molecular electrophosphorescence of the ligand may be observed, as a result of the decay of T_1 to the ligand's ground state, or the nonradiative energy transfer from the T_1 to the resonant levels of the Tb ion, resulting in its narrow characteristic line emissions. An efficient energy transfer from T_1 to Tb ion depends on a closely match (or a little above) of the lower T_1 energy level with the emitting resonance energy levels of the Tb ion. As shown in Fig. 3, our results indicate that the T_1 level of the TDZP excited electrically is a little bellows the resonant levels of

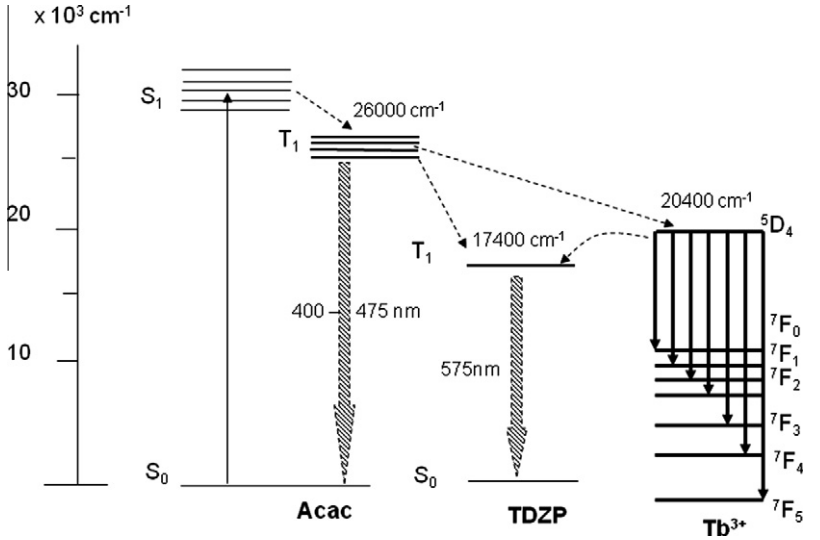

Fig. 3. Energy transfer mechanism in the $Tb(ACAC)_3TDZP$ after excitation.

the Tb ion, resulting in the electrophosphorescence of the TDZP.

To support the speculation that the 580 nm broad band observed on the EL spectra for Device I originates from the ligands, Device II was fabricated with the same architecture as Device I, except that the Tb was replaced with Gd ions in the complex. It is well known that in the case of the Gd ion there is no emission in the first excited state as this lies far above the triplet levels of any matrix or ligand commonly used, thus forcing the decay of the ligands.

The EL spectrum of Device II presented in Fig. 4 shows the same broad bands as Device I, with the 435 nm band being due to the NPB layer. The inversion of the band intensities may be related to a new calibration of the deposition system which occurred during the processes and probably altered the thickness of the organic layers. Nevertheless, since no emission is expected from the Gd(III) ion, it is possible to assume that the 580 nm emission arises from the organic ligands. As far as we know, there are no reports in the literature associating this band to the ACAC ligand and therefore it seems to be mostly related to the TDZP ligand. Moreover, this band was not observed in the PL confirming an efficient energy transfer from the ligands to the Tb ion.

It is well known that rare earth complexes may present a decrease in luminescence intensity due to a variety of mechanisms involving nonradiative loss of energy [2,24]. The lack of the characteristic Tb lines in the electroluminescence spectrum of Device I may be associated with a direct energy transfer of the triplet states of the TDZP ligand to neighboring complexes due to their proximity, instead of transferring the energy to the central Tb ion.

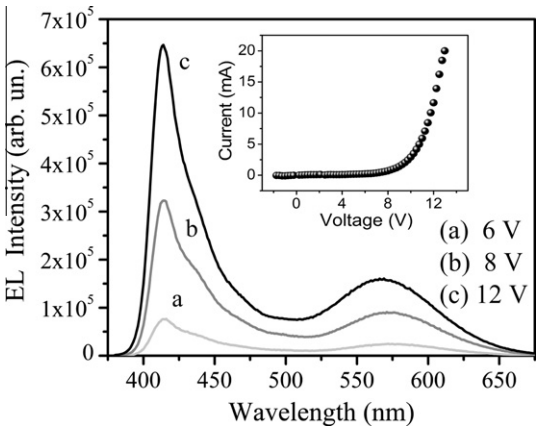

Fig. 4. EL spectra of the Device II as a function of bias voltage. The inset shows the $I \times V$ curve of this device.

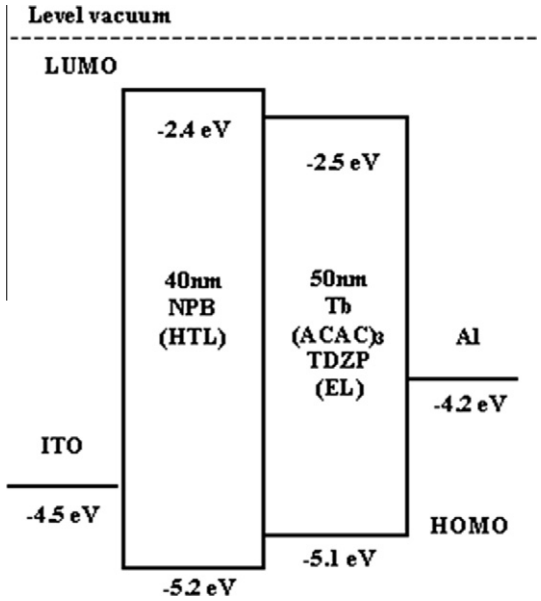

Fig. 5. Rigid band diagram for Device I.

According to the rigid band diagram for Device I (Fig. 5), the HOMO of the $Tb(ACAC)_3TDZP$ complex has a value of 5.1 eV [22]. This level is therefore 0.6 eV below the ITO energy level. Moreover, there is a barrier of around 1.7 eV between the Al energy level and the LUMO of the $Tb(ACAC)_3TDZP$ complex. These differences suggest that in Device I the holes are injected in a more efficient way than the electrons, causing an unbalance of charges in this device.

Several studies have shown that the device efficiency can be increased by using β-diketone rare earth complexes acting as the dopant in the emitting layer, minimizing the quenching mechanism in the devices [25–28]. Thus, we decided to fabricate OLEDs varying the concentration of the $Tb(ACAC)_3TDZP$ complex (as a dopant) in a CBP host matrix. In this way, it is possible to find the best concentration for the rare earth complex allowing the optimization of Device I. In addition, in the new architecture a thin CuPc layer was also introduced.

Fig. 6 shows the EL spectra of the doped Devices III–VI, where the Tb(III) complex concentration varied from 5% to 30% within the CBP matrix. It is expected that by increasing the distance between the complex molecules, decreasing the concentration, the mechanisms involving nonradiative energy loss may also decrease. For the Tb(III) complex concentration of 30% the characteristic Tb(III) lines are weakly visible, but they become more pronounced as the concentration is reduced, resulting in a displacement of the dominant wavelength in the region of green light, as can be seen in the CIE diagram of Fig. 7. From the EL spectra we observe that Device V is the best compromise to obtain a greenish emission, although not with the same degree of purity. The concentration of 7.6% of Tb(III) complex was therefore chosen as the most suitable to perform a device optimization. In this device the broad bands are still visible due to the NPB, at around 435 nm, and at least one other band probably due to the TDZP.

The trapping process imposed by the CBP matrix enables a better control of the recombination region in the emitting layer of the device and can be considered the main mechanism involved in the EL of this device. Since the LUMO level of the NPB is very closed to that of the Tb(III) complex some carrier trapped in the complex may be released and some of the excitons may be formed in the NPB resulting in their emission. The rigid energy band diagram for this device can be seen in reference [22]. The NPB EL is, therefore, a demonstration that the energy transfer mechanism is not as efficient as expected, featuring undesirable bands on the emission spectrum for this device. Nevertheless, a significant improvement in the EL of the Tb(III) complex in the doped devices was observed compared to Device I.

In the EL process, the exciton energy originating from the direct recombination of holes and electrons is mainly

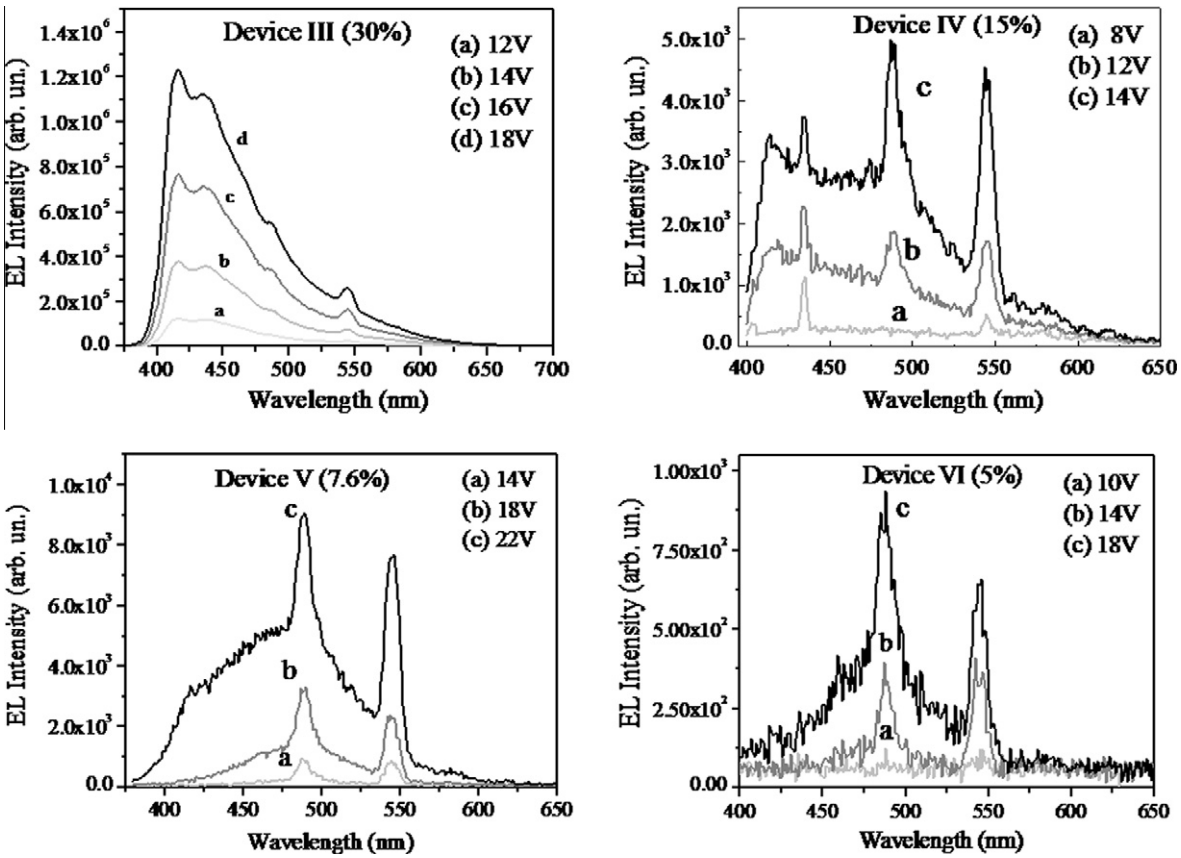

Fig. 6. EL spectra of the doped devices III–VI, where the Tb(III) complex concentration varied from 30% (Device III) to 5% (Device VI) within the CBP matrix.

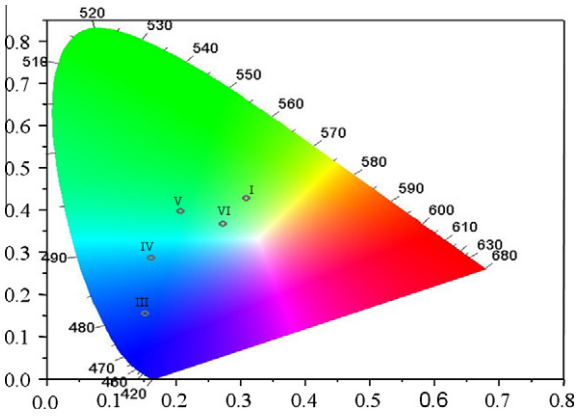

Fig. 7. CIE chromaticity diagram for devices III–VI and Device I, with the respective CIE coordinates: Device III (0.16, 0.16), Device IV (0.17, 0.29), Device V (0.22, 0.40), Device VI (0.29, 0.37), Device I (0.38, 0.43).

absorbed by the ligands, leading to singlet S_1 and triplet T_1 excited states. Meanwhile, a part of the excitons formed within the CBP matrix also gives rise to singlet and triplet excited states. The singlet excited state S_1 of the CBP may decay to the excited singlet state S_1 of the ligands ($S_1 \rightarrow S_1$) through the Forster mechanism [29]. Furthermore, the singlet excited state S_1 of the ligands can decay to its triplet excited state T_1 ($S_1 \rightarrow T_1$), through intersystem crossing (ISC). The T_1 state of the ligands can then decay nonradiatively to the triplet excited state T_1 of CBP through the Dexter mechanism [30] or it can decay through an intra-molecular energy transfer (ET) to the excited state $^5D_4$ of the Tb central ion, originating the narrow spectral lines corresponding to the $^5D_4 \rightarrow {}^7F_j$ ($j = 0,1,2,3,4,5$) transitions. This process is schematically shown in Fig. 8. In addition, the electrophosphorescence of the ligands due to the radiative decay ($T_1 \rightarrow S_0$) can also be present.

Our results demonstrate that the best color purity in the EL emission is obtained with a Tb complex concentration of around 7.6% in the CBP matrix (Device V). This value is comparable with the optimum for the $Ir(ppy)_3$ complex

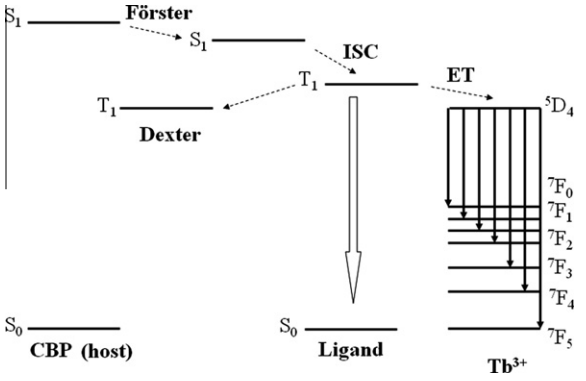

Fig. 8. Scheme of the energy transfer mechanism of the $Tb(ACAC)_3TDZP$ as a dopant in the CBP matrix. S_0 ground state, S_1 excited singlet state, T_1 excited triplet state, ISC = intersystem crossing, ET = energy transfer, Förster and Dexter refer to the type of transfer process taking place as indicated by the arrows.

in the same CBP matrix [31]. Also, in the Tb complex the triplet–triplet exciton annihilation [32] probably plays a crucial role in establishing the doping level. Further investigation is necessary to clarify this point. To improve the device emission quality different experiments were performed modifying the layer thickness and changing some aspects of the OLED architecture. Finally, the best results were obtained when the NPB was replaced by the compound 1-(3-methylphenyl)-1,2,3,4 tetrahydroquinoline-6-carboxyaldehyde-1,1′-diphenylhydrazone (MTCD) (Device VII), which is known not to present EL in the visible region [33].

Fig. 9 shows the EL spectrum of Device VII where the improvement in the emission quality is evident, with the characteristic Tb narrow lines well defined with respect to Device V. The EL spectrum of this device is very similar to the PL spectrum of the Tb complex (Fig. 1), except for the existence of a broad band at around 475 nm, which can be assigned to the electrophosphorescence of the ACAC ligand [34]. To confirm this assignment a new device (Device VIII) was produced. This OLED has the same structure as Device VII, but the $Gd(ACAC)_3TDZP$ complex is used as the dopant, replacing Tb. The EL of Device VIII is shown in the inset of Fig. 9 confirming the nature of the broad band at 475 nm. The electrophosphorescence mechanism of the ACAC ligand obeys the process described in Fig. 8, where in the last stage, the triplet excited state T_1 of the ACAC decays radiatively to its ground singlet state S_0 ($T_1 \rightarrow S_0$).

Finally, in order to compare quantitatively the characteristics of devices I and VII, we present the brightness and the current density of both devices as a function of the voltage, as well as, the current efficiency. In Fig. 10a it is possible to see that the operational voltages of the Device VII are practically two times higher compared to the ones of the Device I, in addition, the brightness intensity of the Device VII is almost four times smaller than the one of the Device I at the same applied voltage. Fig. 10b shows the current efficiency as a function of the current density of both devices, where it is clear that the current efficiency of the Device I is about four times higher than the one of the Device VII. So, the optimization presented here contributed positively only in the aspect of color, where with the Device VII we obtained a gain in the green

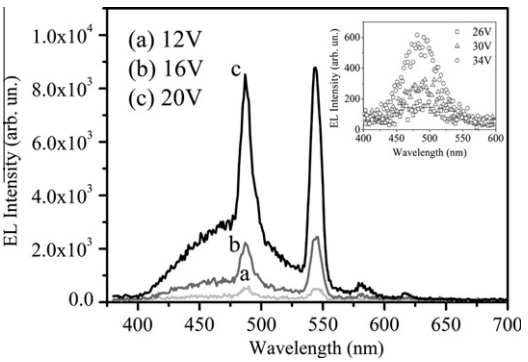

Fig. 9. EL spectra of Device VII as a function of bias voltage. The inset shows the EL of Device VIII where $Gd(ACAC)_3TDZP$ replaced $Tb(ACAC)_3TDZP$ confirming the nature of the broad band at 490 nm.

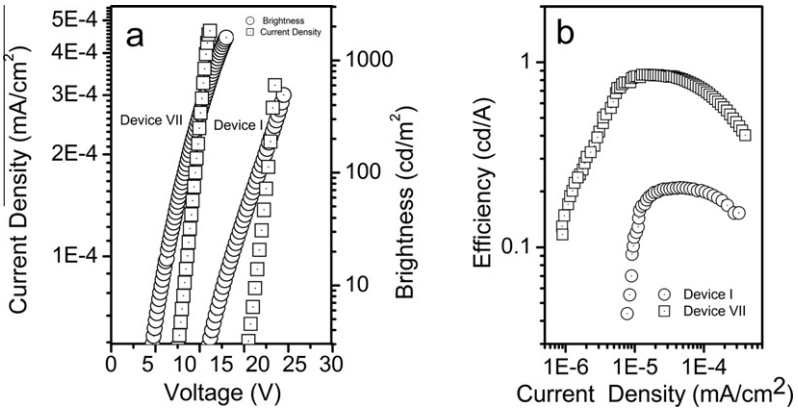

Fig. 10. Working parameters of the devices I and VII. (a) brightness and current density of as a function of the bias voltage; (b) current efficiency as a function of the current density.

Table 1
EL performance of the Device I and the Device VII.

Device	Maximum QE		Maximum brightness			Turn off voltage
	mA/cm^2	cd/A	cd/m^2	mA/cm^2	*V*	
I	13.98	0.86	1673.13	454.28	16.00	16.90
VII	44.57	0.21	491.83	321.23	23.49	23.50

emission purity by starting with the orange emission of Device I, but the other working parameters of the Device VII are less efficient. Table 1 summarizes the EL maximum performance parameters of the devices I and VII. It is clear that a further optimization is needed to increase the efficiency of our Tb complex and to avoid the TDZP emission, which is still present. Moreover, our system presented satisfactory emission properties if compared with the results of references [15–17].

4. Conclusions

In this study the energy transfer mechanism in the new $Tb(ACAC)_3TDZP$ complex used in the fabrication of OLEDs was investigated and discussed. The study showed that bi-layer devices fabricated with the Tb(III) complex used as the emitting layer have low efficiency energy transfer from the organic ligand to the rare earth central ion. In this case, the electroluminescence does not present the characteristic Tb narrow lines, but rather broad bands due to the NPB layer and the ligand electrophosphorescence. Devices using a structure with a co-deposited CBP:Tb(III) complex layer have considerably improved energy transfer and emission color purity allowing the appearance of the Tb(III) lines. In these OLEDs the best concentration of Tb(III) complex in CBP was 7.6% with NPB replaced by MTCD as a hole transporting layer.

Acknowledgements

We thank the following institutions for financial support: CAPES, CNPq, FAPESC, INCT/INEO and INCT-Catalise.

References

[1] J. Kido, Y. Okamoto, Chem. Rev. 102 (2002) 2537.
[2] C. Adachi, M.A. Baldo, S.R. Forrest, J. Appl. Phys. 87 (2000) 8049.
[3] W.G. Quirino, C. Legnani, R. Dos Santos, K. Teixeira, M. Cremona, M. Guedes, H.F. Brito, Thin Solid Films 1096 (2008) 517.
[4] A.A. Vieira, R. Cristiano, A.J. Bortoluzzi, H. Gallardo, J. Mol. Struct. 875 (2008) 364.
[5] R. Cristiano, H. Gallardo, A.J. Bortoluzzi, H.I. Bechtold, C.E.M. Campos, R.L. Longo, Chem. Commun. 41 (2008) 5134.
[6] R. Cristiano, D.M.P.D. Santos, G. Conte, H. Gallardo, Liq. Cryst. 33 (2006) 997.
[7] H. Burroughes, D.D.C. Bradley, A.R. Brown, R.N. Marks, K. Mackay, R.H. Friend, P.L. Burns, A.B. Holmes, Nature 347 (1990) 539.
[8] G. Blasse, B.C. Grabmaier, Luminescence Materials, Springer Verlag, Heildeberg, 1994.
[9] A.A.S. Araujo, H.F. Brito, O.L. Malta, J.R. Matos, E.E.S. Teotonio, S. Storpirtis, C.M.S. Izumi, J. Inorg. Biochem. 88 (2002) 87.
[10] M.A. Baldo, D.F. O'Brien, M.E. Thompson, S.R. Forrest, Phys. Rev. B. 60 (1999) 14422.
[11] J.R. Sheats, H. Antoniadis, M. Hueschen, W. Leonard, J. Miller, R. Moon, D. Roitman, Stocking Sci. 273 (1996) 884.
[12] M.P. Bemquerer, C. Bloch, H.F. Brito, E.E.S. Teotonio, M.T.M. Miranda, J. Inorg. Biochem. 91 (2002) 363.
[13] I. Hemmila, V. Laitala, J. Fluoresc. 15 (2005) 529.
[14] C. Adachi, M.A. Baldo, M.E. Thompson, S.R. Forrest, J. Appl. Phys. 90 (2001) 5048.
[15] J. Kido, K. Nagai, Y. Ohashi, Chem. Lett. 657 (1990).
[16] Y. Zheng, J. Lin, Y. Liang, Q. Lin, Y. Yu, Q. Meng, Y. Zhou, S. Wang, H. Wang, H. Zhang, J. Mater. Chem. 11 (2001) 2615.
[17] Y. Zheng, J. Lin, Y. Liang, Q. Lin, Y. Yu, C. Guo, S. Wang, H. Zhang, Mat. Lett. 54 (2002) 424.
[18] H. Gallardo, G. Conte, P. Tuzimoto, A. Bortoluzzi, R.A. Peralta, A. Neves, Inorg. Chem. Comm. 11 (2008) 1292.
[19] S.J. Yeh, M.F. Wu, C.T. Chen, Y.H. Song, Y. Chi, M.H. Ho, S.F. Hsu, C.H. Chen, Adv. Mater. 17 (2005) 285.
[20] S.R. Forrest, J.J. Brown, M.E. Thompson, Appl. Phys. Lett. 82 (2003) 2422.
[21] H. Gallardo, G. Conte, A.J. Bortoluzzi, Synthesis 23 (2006) 3945.
[22] H. Gallardo, G. Conte, A.J. Bortoluzzi, I.H. Bechtold, A. Pereira, M. Cremona, C. Legnani, W.G. Quirino, Inorg. Chim. Acta 365 (2011) 152.
[23] R. Reyes, M. Cremona, E.E.S. Teotonio, H.F. Brito, O.L. Malta, Thin Solid Films 469 (2004) 59.

[24] J. Kalinowski, J. Phys. D 32 (1999) 179.
[25] H. Heil, J. Steiger, R. Schmechel, H. von Seggern, J. Appl. Phys. 90 (2001) 5357.
[26] P.P. Sun, J.P. Duan, H.T. Shih, C.H. Cheng, Appl. Phys. Lett. 81 (2002) 792.
[27] Z.R. Hong, C.J. Liang, R.G. Li, W.L. Li, D. Zhao, D. Fan, D.Y. Wang, B. Chu, F.X. Zang, L.S. Hong, S.T. Lee, Adv. Mater. 13 (2001) 1241.
[28] J. Kido, H. Hayase, K. Hongawa, K. Nagai, K. Okuyama, Appl. Phys. Lett. 65 (1994) 2124.
[29] T. Forster, Disc. Faraday Soc. 27 (1959) 17.
[30] D.L. Dexter, J. Chem. Phys. 21 (1953) 836.
[31] S. Lamansky, P. Djurovich, D. Murphy, F. Adbel-Razzaq, H.-E. Lee, C. Adachi, P.E. Burrows, S.R. Forrest, M.E. Thompson, J. Am. Chem. Soc. 123 (2001) 4304.
[32] S. Reineke, G. Schwartz, K. Walzer, K. Leo, Phys. Status Solidi Rapid Res. Lett. 3 (2009) 67.
[33] W.G. Quirino, C. Legnani, M. Cremona, P.P. Lima, S.A. Junior, O.L. Malta, Th. Sol. Films 23 (2006) 494.
[34] William R. Dawson, John L. Kropp, Maurice W. Windsor, J. Chem. Phys, 45 (1966) 2410.